Covariant Chu–Kovasznay Decomposition: Resolving Thermodynamic Ambiguity in Compressible Flows

Chanho Park,[1] Gyeongho Gong,[1] Yeachan Kwak,[1] and Seongim Choi[1]

[1] *School of Mechanical Engineering, Gwangju Institute of Science and Technology, Gwangju 61005, Republic of Korea*

We establish the Covariant Chu–Kovasznay Decomposition (CCKD), a geometric framework that resolves thermodynamic ambiguity in compressible mode content by formulating the decomposition on the effective acoustic spacetime. Enforcing orthogonality in the covariant Chu energy norm, we show that shock–turbulence interaction, often treated as a scattering source, is, in the idealized linear, inviscid setting, a near-unitary (Chu-isometric) scattering map constrained by conservation of covariant Chu-energy flux. In the canonical Shu-Osher problem, CCKD characterizes the shock as a thermo-acoustic lens, mathematically demonstrating that the transfer of entropy fluctuations into sound follows a geometric blue-shift ($k_{\text{out}} = \Lambda k_{\text{in}}$) analogous to gravitational blue-shift. Thus, while the mean flow produces entropy across the shock, the fluctuation mapping is information-preserving on the retained subspace; practical information loss arises from noise, truncation, and model mismatch, not shock physics.

Introduction— Separating acoustic, vortical, and thermodynamic fluctuations in compressible flows is a foundational step in aeroacoustics [1–5], combustion instability [6–8], and the analysis of shock–turbulence interaction (STI) [9–11]. Yet, downstream measurements in these regimes are often plagued by an intrinsic ambiguity between physical fluctuations and geometric coordinate effects [12–17]. Classical mode decompositions trace back to Kovasznay's linear splitting [18] and subsequent energetics-based formulations, such as Chu's disturbance energy [19] and Morfey's acoustic energy flux [20], or the momentum potential variables [21], that clarify how entropy and vorticity can masquerade as sound under naive post-processing. However, this ambiguity becomes acute near strong inhomogeneities, such as shocks, thermal lenses, and transcritical flows, where the effective acoustic geometry is curved [22–24]. In such regimes, standard Euclidean projections are no longer invariant to the underlying metric structure, potentially leading to ambiguous definitions or interpretation artifacts [25–30].

A practical symptom is geometric leakage: curvature-induced kinematic signatures are misidentified as physical vorticity or acoustic energy when operators are defined in flat space [27, 31]. Motivated by the acoustic-metric viewpoint [32–35], we build a covariant decomposition whose orthogonality and energetics are defined by the same geometry that governs wave propagation. Specifically, the proposed Covariant Chu–Kovasznay Decomposition (CCKD) extends our kinematic CHHD framework [36] by incorporating (i) compressible modal structure (Chu–Kovasznay variables) and (ii) the Chu-energy inner product as the metric-consistent notion of amplitude and orthogonality. In the nonuniform limit, CCKD recovers the familiar Euclidean decomposition; in strongly curved or near-degenerate regimes, it remains well-posed because the projectors are intrinsic to the acoustic spacetime.

Beyond robust mode separation, a covariant energetic formulation reframes shock-generated noise, classically treated as a volumetric source term [37], as a deterministic scattering process. For a steady normal shock, within the inviscid linearized theory on the retained fluctuation subspace, conservation of energy flux, inherent to the linearized Rankine-Hugoniot relations [9], implies that the cross-shock map acts as an isometric scattering operator on the covariant subspace. This perspective motivates shock-wave holography: upstream thermodynamic structure is not destroyed, but is deterministically re-encoded into downstream propagating acoustic content via a predictable geometric blue-shift [38]. Physically, the shock behaves as a thermo-acoustic lens that performs a systematic spectral relabeling and amplification, formally analogous to the gravitational blueshift of signals propagating into a potential well [39–41]. This yields a crucial duality: while the mean state exhibits irreversible entropy production, the fluctuation dynamics preserves the Shannon information carried by the retained modes. Consequently, the upstream state can, in principle, be reconstructed from downstream observations via an inverse-scattering law [42, 43], converting the apparent noise back into the underlying signal.

In this Letter, we establish the Covariant Chu–Kovasznay Decomposition (CCKD) as a geometric framework for resolving thermodynamic ambiguity in curved acoustic spacetimes. We first validate the framework's geometric robustness using a thermal lens and an analogue black hole [44–46], demonstrating clean mode separation even near coordinate singularities. We then apply it to the canonical Shu–Osher problem [47–49] to substantiate the unitary scattering physics, enabling the blind holographic reconstruction of upstream entropy via the predicted geometric blue-shift [38, 39].

Acoustic geometry and the chu energy norm— Let $\Omega \subset \mathbb{R}^d$ be the spatial domain. We consider a stationary, inhomogeneous background state $\mathbf{q}_0 = (\rho_0, p_0, \mathbf{U}_0)^\top$. The propagation of fluctuations $\mathbf{q}' \equiv (s', p', \mathbf{u}')^\top$ is governed by the effective acoustic metric γ_{ij}. Here $\rho_0(x)$, $p_0(x)$, and $\mathbf{U}_0(x)$ denote the background density, pres-

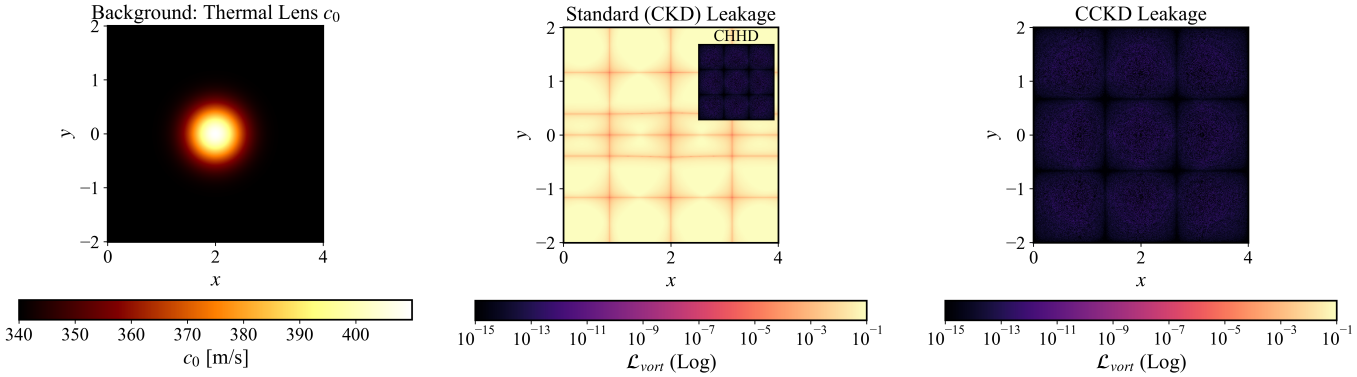

(a) Background thermal lens $c_0(\mathbf{x})$.

(b) Standard (Euclidean) leakage magnitude.

(c) Covariant (metric-aligned) leakage magnitude.

FIG. 1: Kinematic validation: Vorticity isolation in a thermal lens. A refractive background bends rays without creating true vorticity. Euclidean post-processing misinterprets curvature as solenoidal content; the covariant projection suppresses this geometric leakage.

sure, and velocity fields, respectively. Thermodynamics is closed by an equation of state, and s denotes the specific entropy; primes indicate perturbations about the background (e.g., $p' = p - p_0$, $\mathbf{u}' = \mathbf{u} - \mathbf{U}_0$). In Cartesian coordinates, the inverse metric is defined by the background kinematics as $\gamma^{ij} \equiv \delta^{ij} - U_0^i U_0^j / c_0^2$, with $\gamma_{ij} \equiv (\gamma^{ij})^{-1}$. To ensure coordinate invariance, differential operators are defined via the Levi-Civita connection compatible with γ. The covariant gradient ∇_γ, divergence $\nabla_\gamma \cdot$, and Laplace–Beltrami operator Δ_γ are given by

$$(\nabla_\gamma \phi)^i \equiv \gamma^{ij} \partial_j \phi, \qquad \nabla_\gamma \cdot \mathbf{v} \equiv \frac{1}{\sqrt{\gamma}} \partial_i \big(\sqrt{\gamma} v^i\big), \\ \Delta_\gamma \phi \equiv \nabla_\gamma \cdot (\nabla_\gamma \phi), \tag{1}$$

where $\gamma \equiv \det(\gamma_{ij})$, so that $\sqrt{\gamma} = \sqrt{\det(\gamma_{ij})}$, and the consistent integration measure is $dV_\gamma \equiv \sqrt{\gamma}\, d^d x$. We also define the γ-inner product on contravariant vectors by $\langle \mathbf{a}, \mathbf{b} \rangle_\gamma \equiv \gamma_{ij} a^i b^j$.

To rigorously define modal orthogonality, we employ the Covariant Chu Energy Inner Product [19]. This choice is physically motivated: it extends the classical acoustic energy density to inhomogeneous, shearing (and reacting) backgrounds in a coordinate-invariant manner. The inner product is defined as

$$\langle \mathbf{q}'_a, \mathbf{q}'_b \rangle_{\mathrm{Chu}} \equiv \int_\Omega \Bigg(\underbrace{\frac{\rho_0 T_0}{c_p} s'_a s'_b}_{\text{Thermal}} + \underbrace{\frac{p'_a p'_b}{\rho_0 c_0^2}}_{\text{Compressive}} \\ + \underbrace{\rho_0 \gamma_{ij} u'^i_a u'^j_b}_{\text{Kinetic}} \Bigg) dV_\gamma. \tag{2}$$

In (2), $T_0(x)$ is the background temperature and c_p is the specific heat at constant pressure. We take $s' \equiv \delta s$ as the specific-entropy fluctuation. The background sound speed satisfies $c_0^2 = \kappa p_0 / \rho_0$ with $\kappa \equiv c_p / c_v$ the ratio of specific heats. For an ideal gas, $T_0 = p_0/(\rho_0 R)$; in nondimensional units with $R = 1$, this reduces to $T_0 = p_0/\rho_0$. The associated norm $\|\mathbf{q}'\|^2_{\mathrm{Chu}}$ corresponds to the total disturbance energy of the linearized system. Consequently, orthogonality in this norm guarantees energy additivity across the projected subspaces, so that apparent mode coupling arises from dynamics rather than from the projection.

Decomposition algorithm— We construct the decomposition $\mathbf{q}' = \mathbf{q}'_S + \mathbf{q}'_\Omega + \mathbf{q}'_P$ by sequentially projecting the state vector onto mutually orthogonal subspaces.

Step 1: Thermodynamic projection. We first isolate the non-propagating entropic subspace. Because the Chu metric in Eq. (2) is block-diagonal with respect to entropy and mechanics, we define the entropy mode as

$$\mathbf{q}'_S \equiv (s',\, 0,\, \mathbf{0})^\top. \tag{3}$$

By construction, $\langle \mathbf{q}'_S, \mathbf{q}'_{\Omega/P} \rangle_{\mathrm{Chu}} \equiv 0$ for any modes with vanishing entropy.

Step 2: Covariant Helmholtz decomposition. The mechanical subspace is split by decomposing the velocity field $\mathbf{u}' = \mathbf{u}'_P + \mathbf{u}'_\Omega$. The acoustic (potential) velocity $\mathbf{u}'_P$ is defined as the covariant gradient of a scalar potential, $\mathbf{u}'_P \equiv \nabla_\gamma \phi$. To ensure $\mathbf{u}'_P$ captures the full compressible characteristic, ϕ is obtained from the variational (weak) covariant Poisson problem:

$$\text{Find } \phi \in H^1(\Omega)/\mathbb{R} \text{ such that} \\ \int_\Omega \langle \nabla_\gamma \phi, \nabla_\gamma w \rangle_\gamma \, dV_\gamma \\ = \int_\Omega \langle \mathbf{u}', \nabla_\gamma w \rangle_\gamma \, dV_\gamma \\ \forall\, w \in H^1(\Omega). \tag{4}$$

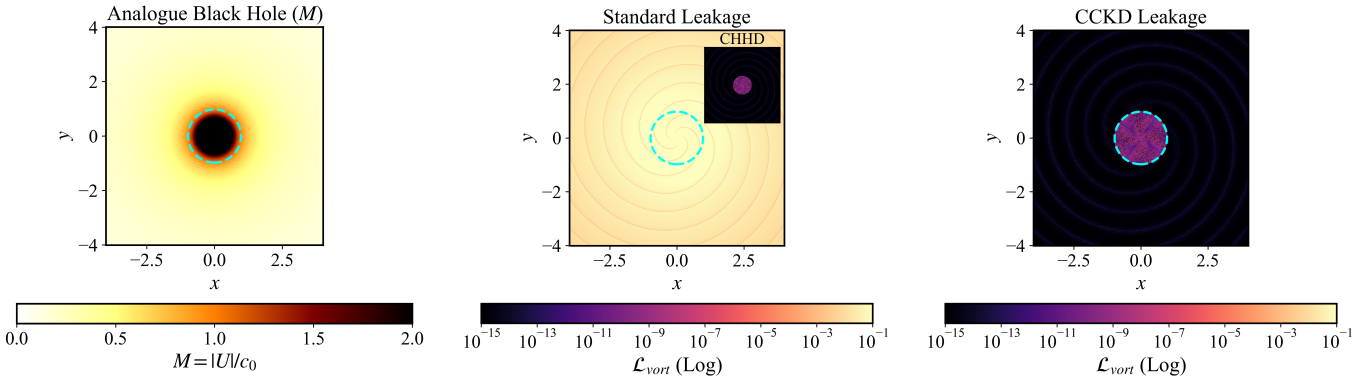

(a) Analogue BH background (Mach number M).

(b) Standard (Euclidean) vorticity leakage.

(c) Covariant vorticity leakage.

FIG. 2: Geometric leakage near an analogue black hole. A horizon geometry amplifies Euclidean projection errors, identifying curvature as vorticity. The covariant projection suppresses this artifact, with residual leakage confined to the regularized interior (inside the horizon).

where $\mathbf{u}'$ is interpreted as a contravariant vector field in the γ-inner product. The solution is unique up to an additive constant, which we fix by enforcing $\int_\Omega \phi \, dV_\gamma = 0$. The vortical velocity is then the solenoidal residual $\mathbf{u}'_\Omega \equiv \mathbf{u}' - \mathbf{u}'_P$, satisfying $\nabla_\gamma \cdot \mathbf{u}'_\Omega = 0$. Equivalently, $\mathbf{u}'_P$ is the γ-orthogonal projection of $\mathbf{u}'$ onto gradient fields, obtained by minimizing

$$\mathcal{K}[\mathbf{v}] = \int_\Omega \gamma_{ij} v^i v^j \, dV_\gamma, \tag{5}$$

which ensures kinematic orthogonality under the acoustic metric, i.e., $\int_\Omega \gamma_{ij} u'^i_P u'^j_\Omega \, dV_\gamma = 0$.

Step 3: Hydrodynamic pressure balance. Finally, the pressure is decomposed as $p' = p'_P + p'_\Omega$. The vortical (pseudo-sound) pressure p'_Ω is defined to balance the vortical mode's convective acceleration against the background flow. This isolates the hydrodynamic footprint supported by the mean shear from the unsteady acoustic fluctuations. Taking the covariant divergence of the linearized momentum equation yields the variational constraint:

$$\begin{aligned} &\text{Find } p'_\Omega \in H^1(\Omega)/\mathbb{R} \text{ such that} \\ &\int_\Omega \langle \nabla_\gamma p'_\Omega, \nabla_\gamma w \rangle_\gamma \, dV_\gamma \\ &\quad = \int_\Omega \langle \rho_0 (\mathbf{U}_0 \cdot \nabla_\gamma) \mathbf{u}'_\Omega, \nabla_\gamma w \rangle_\gamma \, dV_\gamma \\ &\forall \, w \in H^1(\Omega). \end{aligned} \tag{6}$$

The homogeneous Neumann condition is natural and is satisfied weakly by (6); uniqueness is fixed by enforcing the zero-mean gauge $\int_\Omega p'_\Omega \, dV_\gamma = 0$.

Crucially, the convective term $(\mathbf{U}_0 \cdot \nabla_\gamma)\mathbf{u}'_\Omega$ incorporates the acoustic metric's Levi-Civita connection via the Christoffel symbols, $\Gamma^k_{ij} = \frac{1}{2}\gamma^{km}(\partial_i \gamma_{jm} + \partial_j \gamma_{im} - \partial_m \gamma_{ij})$. The resulting derivative, $U_0^j(\partial_j u'^{\,k}_\Omega + \Gamma^k_{jm} u'^{\,m}_\Omega)$, correctly captures inertial forces arising from effective geometric curvature (e.g., strong refraction), ensuring that metric-induced bending is not misidentified as an acoustic source.

In all validations reported here, we employ this natural (Neumann) variational formulation (6) together with the zero-mean gauge for consistency with the discrete covariant operators. The acoustic pressure is the residual $p'_P \equiv p' - p'_\Omega$. With the mode vectors defined as $\mathbf{q}'_\Omega \equiv (0, p'_\Omega, \mathbf{u}'_\Omega)^\top$ and $\mathbf{q}'_P \equiv (0, p'_P, \mathbf{u}'_P)^\top$, the construction ensures that cross terms vanish in the inner product. Consequently, the CCKD basis diagonalizes the covariant energy norm:

$$\|\mathbf{q}'\|^2_{\text{Chu}} = \|\mathbf{q}'_S\|^2_{\text{Chu}} + \|\mathbf{q}'_\Omega\|^2_{\text{Chu}} + \|\mathbf{q}'_P\|^2_{\text{Chu}}. \tag{7}$$

In our implementation, the variational problems (4) and (6) are discretized using symmetric weak-form (stiffness) operators constructed from discrete adjoints, so the projection identities hold to the numerical noise floor.

Kinematic validation (refraction-induced vorticity leakage in a thermal lens)— We first validate kinematic mode isolation using an acoustic perturbation propagating through a stationary refractive background. This thermal-lens benchmark contains strong spatial variation in $c_0(\mathbf{x})$ but no physical mechanism to generate vorticity; therefore, the true acoustic mode remains (covariantly) irrotational. The test isolates a well-known failure mode of Euclidean post-processing: geometric curvature of rays in an inhomogeneous medium can be misinterpreted as solenoidal content, producing spurious vorticity leakage in velocity-only decompositions. Figure 1a shows the background lens $c_0(\mathbf{x})$. A standard Euclidean diagnostic reports substantial vorticity leakage throughout the domain (Fig. 1b), despite the input being vorticity-free in the acoustic manifold sense. In contrast, the covari-

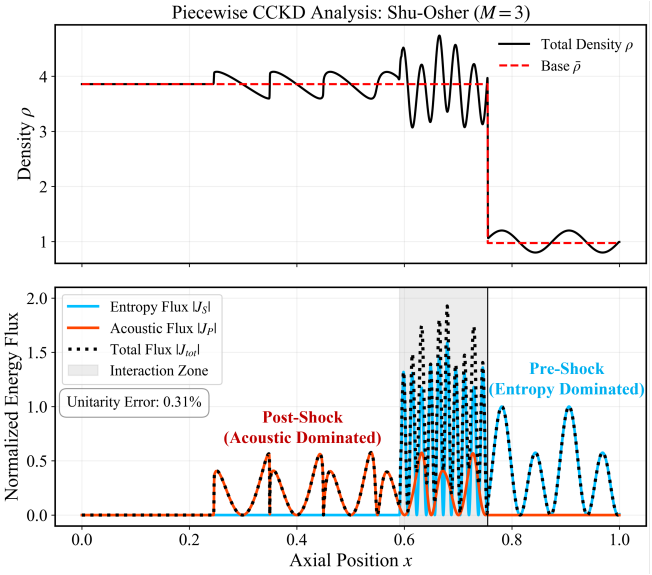

FIG. 3: Shu–Osher benchmark ($M_1 = 3$). Top: density profile of the shock–entropy interaction. Bottom: modal Chu-energy fluxes ($J_{\mathcal{S}}, J_{\mathcal{P}}$) and total flux J_{tot}. The shock redistributes flux from entropic to acoustic while J_{tot} remains anchored to the upstream plateau (defect $\varepsilon_J \approx 0.31\%$), consistent with a passive thermo-acoustic lens.

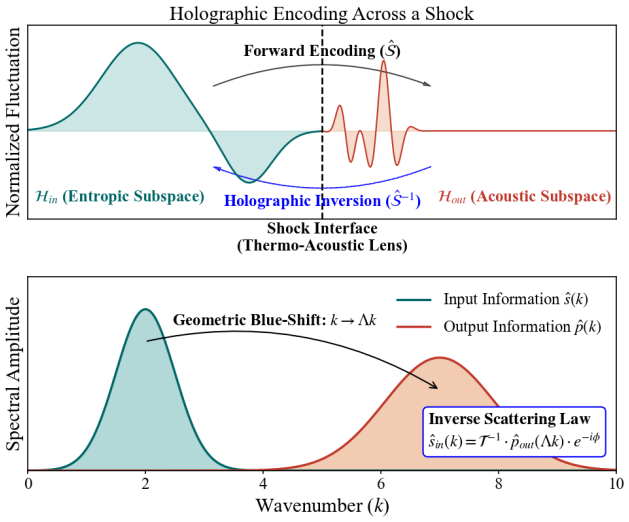

FIG. 4: Shock-wave holography as deterministic scattering. Top: Physical-space view where the shock functions as a thermo-acoustic lens, deterministically encoding upstream entropy into downstream acoustic signatures. Bottom: Fourier-space view illustrating the geometric blue-shift ($k \mapsto \Lambda k$), which establishes an invertible scattering law for exact source reconstruction via transmission and phase factors.

ant projection aligns the decomposition with the effective acoustic metric and suppresses this purely geometric leakage (Fig. 1c), recovering a vanishing kinematic residual up to truncation error.

Kinematic validation (horizon-amplified vorticity leakage in an analogue black hole)— Next, we validate kinematic mode isolation in the most transcritical regime: an analogue black hole formed by a rotating draining vortex, where an acoustic horizon ($|v_r| = c_0$) renders the effective acoustic metric near-degenerate. This geometry provides a stringent stress test for covariant mode separation because strong curvature and spatial contraction the horizon can amplify numerical and coordinate-induced artifacts. Figure 2a shows the background Mach number $M = |\mathbf{U}_0|/c_0$ and the horizon location. A standard Euclidean diagnostic reports substantial vorticity leakage (Fig. 2b), misinterpreting horizon-induced geometric curvature and coordinate distortion as solenoidal content. In contrast, the covariant projection aligns the decomposition with the acoustic manifold and suppresses this purely geometric leakage by orders of magnitude (Fig. 2c), recovering a vorticity-free acoustic mode up to truncation error.

Chu-covariant flux exchange at a shock— We analyze the Shu–Osher configuration (Mach-3 shock–entropy interaction) [47] to formalize deterministic mode conversion. Using the Chu disturbance-energy flux, the physical-space representation of the Chu inner product that underlies our covariant energetics [19], the total disturbance flux decomposes into acoustic and entropic contributions,

$$J_{\mathrm{tot}}(x) \;=\; J_{\mathcal{P}}(x) + J_{\mathcal{S}}(x), \tag{8}$$

defined explicitly using background variables as

$$\begin{aligned} \mathcal{E}_{\mathcal{P}} &= \frac{1}{2}\rho_0 u_{\mathcal{P}}'^2 + \frac{1}{2}\frac{p_{\mathcal{P}}'^2}{\rho_0 c_0^2}, \quad & J_{\mathcal{P}} &= U\mathcal{E}_{\mathcal{P}} + p_{\mathcal{P}}' u_{\mathcal{P}}', \\ \mathcal{E}_{\mathcal{S}} &= \frac{1}{2}\frac{\rho_0 T_0}{c_p}\, s'^2, & J_{\mathcal{S}} &= U\mathcal{E}_{\mathcal{S}}, \end{aligned} \tag{9}$$

where $U(x) = u_0(x) - W_s$ is the shock-relative mean velocity. In the inviscid linear theory, the linearized Rankine–Hugoniot relations [9] impose physical conservation laws across the shock. In the present geometric framework, these constraints imply conservation of the covariant Chu-energy flux, rendering the cross-shock map isometric on the retained subspace. Figure 3 confirms this: incident entropic flux ($J_{\mathcal{S}}$) is converted into acoustic flux ($J_{\mathcal{P}}$) while J_{tot} remains anchored to its upstream plateau with no secular drift. We quantify the residual deviation using the relative conservation defect $\varepsilon_J = \max_x |J_{\mathrm{tot}}(x) - \langle J_{\mathrm{tot}}\rangle_{\mathrm{pre}}| / \max_x |J_{\mathrm{tot}}(x)|$, obtaining $\varepsilon_J \approx 0.31\%$, a value attributable to discretization rather than physics [48]. The shock therefore functions as a passive thermo-acoustic lens, deterministically exchanging energy between subspaces while conserving total Chu flux.

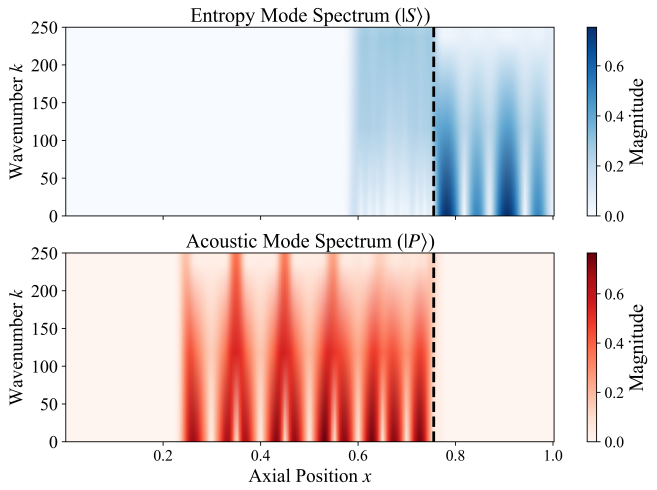

FIG. 5: Spectral signature of near-isometric scattering. Top: Incident entropy mode $|S\rangle$ dominated by low-wavenumber content. Bottom: Scattered acoustic mode $|P\rangle$ exhibiting a distinct spectral blue-shift at the shock interface ($x \approx 0.75$). Here the ket notation denotes the modal coefficient vectors in the chosen spectral basis. This frequency up-conversion indicates the shock functions as a compressive thermo-acoustic lens, mathematically analogous to a gravitational blue-shift.

Covariant perspective: Holographic encoding via thermo-acoustic lens— Reframing the classical conservation laws of LIA [50], we propose that the shock acts as a deterministic thermo-acoustic lens (Fig. 4), encoding upstream entropy into downstream acoustic waves. Under this framework, geometric consistency becomes paramount. Any decomposition lacking metric compatibility, specifically Euclidean HHD in curved acoustic spacetimes, generates spurious energy leakage. This artifact effectively acts as noise, degrading the scattering map's invertibility and obscuring the underlying unitary physics.

The structural constraint underpinning this map is the conservation of covariant Chu-energy flux, $J^{\text{out}}_{\text{tot}} = J^{\text{in}}_{\text{tot}}$. Crucially, this conservation applies to the evolution of fluctuations on the acoustic metric and is logically distinct from the thermodynamic entropy jump ($\Delta s > 0$) of the background mean flow. Consequently, on the retained fluctuation subspace, the cross-shock mapping constitutes a norm-preserving (unitary) operator in the Chu metric. This implies that any information loss is not intrinsic to shock physics, but arises solely from practical limitations such as measurement noise, modal truncation, or model mismatch [51, 52].

Physically, this structure is realized through a deterministic spectral compression, as evidenced by the spectral evolution in Fig. 5. As the entropy wave crosses the shock, it is converted into an acoustic wave via a geometric blue-shift, $k_{\text{out}} = \Lambda k_{\text{in}}$, where $\Lambda \equiv k_{\text{out}}/k_{\text{in}} > 1$ is the geometric blue-shift factor relating the downstream acoustic wavenumber to the incident upstream entropy wavenumber. As derived in Appendix C, this scaling corresponds physically to the Doppler shift induced by the convective velocity jump; however, in the covariant framework, it is intrinsic to the relativistic acoustic geometry, mathematically analogous to the gravitational blue-shift of a photon falling into a potential well [39–41]. Just as a gravitational well compresses the wavelength of light without erasing its phase relations, the shock deterministically transfers upstream thermodynamic structure into a high-frequency acoustic carrier.

Information capacity and holographic reconstruction— To quantify the information capacity of this channel, we adopt a stochastic channel model. Let the upstream entropy state $\mathbf{x} \in \mathbb{C}^N$ (with N the number of retained modes) be drawn from a maximum-entropy ensemble $\mathbf{x} \sim \mathcal{CN}(\mathbf{0}, \mathbf{S}_x)$, where $\mathcal{CN}$ denotes a circularly symmetric complex Gaussian and $\mathbf{S}_x$ is its covariance. The state is observed via the discretized scattering map $\mathbf{A}$ as $\mathbf{y} = \mathbf{A}\mathbf{x} + \mathbf{n}$, where $\mathbf{n} \sim \mathcal{CN}(\mathbf{0}, \mathbf{S}_n)$ is additive noise with covariance $\mathbf{S}_n$. We assume the noise is white in a Chu-orthonormal basis, i.e., in a basis orthonormal under $\langle\cdot,\cdot\rangle_{\text{Chu}}$ we have $\mathbf{S}_n = \sigma_n^2\mathbf{I}$. The extractable information is quantified by the Shannon mutual information $I(\mathbf{x};\mathbf{y}) = h(\mathbf{y}) - h(\mathbf{y}|\mathbf{x})$ [52], where $h(\cdot)$ denotes differential entropy. Expressing the scattering operator $\mathbf{A}$ via its singular value decomposition $\mathbf{A} = \mathbf{U}\mathbf{\Sigma}\mathbf{V}^\dagger$, where $(\cdot)^\dagger$ denotes the Hermitian transpose, $\mathbf{U}, \mathbf{V}$ are unitary, and $\mathbf{\Sigma} = \text{diag}(\sigma_i)$, the mutual information is determined by the singular spectrum $\{\sigma_i\}$:

$$I(\mathbf{x};\mathbf{y}) = \sum_{i=1}^{N} \log_2\left(1 + \text{SNR}_i \cdot \sigma_i^2\right), \tag{10}$$

where SNR_i is the signal-to-noise ratio in the i-th eigenmode.

Crucially, the Chu-flux conservation law ($J^{\text{out}}_{\text{tot}} = J^{\text{in}}_{\text{tot}}$) implies that, on the retained fluctuation subspace and up to the measured flux mismatch, the scattering map is approximately isometric in the Chu norm, i.e., $\mathbf{A}^\dagger\mathbf{A} \approx \mathbf{I}$. Consequently, the singular values satisfy $\sigma_i \approx 1$ for the resolved modes. Unlike dissipative dynamics (e.g., viscous decay) or incomplete measurements where $\sigma_i \ll 1$ leads to information loss, the shock primarily performs a lossless mixing/encoding of upstream structure into downstream acoustic degrees of freedom. In the noiseless limit ($\mathbf{n} = \mathbf{0}$) this implies invertibility (full rank) on the retained subspace, whereas with noise the recoverable information is bounded by (10) and decreases with SNR and model mismatch. We term this inverse capability Shock-wave holography; see, e.g., standard inverse-scattering references [42, 43], and Appendix D for a comprehensive validation of blind reconstruction.

Conclusion—We established the Covariant Chu–

Kovasznay Decomposition (CCKD) as a geometric, coordinate-invariant thermodynamic analogue of Kovasznay theory. Enforcing orthogonality in the covariant Chu energy norm makes the acoustic/entropic split intrinsic to the effective acoustic spacetime, mitigating ambiguities that contaminate Euclidean diagnostics in strongly inhomogeneous flows. We validated CCKD on a thermal-lens entropy spot, an analogue black hole, and Shu–Osher, demonstrating robust mode separation under strong metric curvature and near-horizon degeneracy.

In Shu–Osher, CCKD complements the classical scattering picture: within the linear inviscid model, the shock acts as a thermo-acoustic lens that deterministically redistributes fluctuation energy between subspaces and produces a geometric blue-shift ($k \to \Lambda k$). The associated covariant flux budget closes to within a small finite-resolution mismatch ε_J. Thus, while shocks dissipate the mean flow, the CCKD projection is (near-)isometric in the Chu metric, and practical information loss is dominated by numerical/measurement noise, truncation, and model/discretization mismatch rather than geometric mode mixing. In the analogue-gravity interpretation, horizons behave as geometry-induced focusing elements rather than sources of spurious post-processing artifacts [22, 53, 54].

CCKD therefore replaces kinematic heuristics with a geometry-consistent closure for tracking fluctuation energy on curved acoustic manifolds, and motivates covariant Lighthill-type generalizations. Future work will extend the projection to nonstationary and viscous backgrounds, enabling quantitative accounting of conversion and dissipation beyond the near-isometric limit.

Acknowledgments— The authors sincerely thank Professor Ray-Sing Lin for providing valuable insights regarding the thermodynamic extension of the geometric framework.

[1] M. J. Lighthill, On sound generated aerodynamically I. general theory, Proceedings of the Royal Society of London. Series A. Mathematical and Physical Sciences **211**, 564 (1952).
[2] M. J. Lighthill, On sound generated aerodynamically II. turbulence as a source of sound, Proceedings of the Royal Society of London. Series A. Mathematical and Physical Sciences **222**, 1 (1954).
[3] N. Curle, The influence of solid boundaries upon aerodynamic sound, Proceedings of the Royal Society of London. Series A. Mathematical and Physical Sciences **231**, 505 (1955).
[4] J. E. Ffowcs Williams and D. L. Hawkings, Sound generation by turbulence and surfaces in arbitrary motion, Philosophical Transactions of the Royal Society of London. Series A, Mathematical and Physical Sciences **264**, 321 (1969).
[5] M. E. Goldstein, *Aeroacoustics* (McGraw-Hill, 1976).
[6] S. M. Candel, Combustion instabilities coupled by pressure waves and their active control, Symposium (International) on Combustion **24**, 1277 (1992), twenty-Fourth Symposium on Combustion.
[7] T. Poinsot and D. Veynante, *Theoretical and Numerical Combustion*, 2nd ed. (R.T. Edwards, Inc., Philadelphia, 2005).
[8] S. H. Preetham and T. C. Lieuwen, Response of turbulent premixed flames to harmonic acoustic forcing, Proceedings of the Combustion Institute **31**, 1427 (2007).
[9] H. S. Ribner, *Convection of a Pattern of Vorticity Through a Shock Wave*, Tech. Rep. NACA-TR-1164 (National Advisory Committee for Aeronautics, Washington, D.C., 1954).
[10] Y. Andreopoulos, J. H. Agui, and G. Briassulis, Shock wave–turbulence interactions, Annual Review of Fluid Mechanics **32**, 309 (2000).
[11] S. Pirozzoli, Numerical methods for high-speed flows, Annual Review of Fluid Mechanics **43**, 163 (2011).
[12] S. C. Crow, Aerodynamic sound emission as a singular perturbation problem, Studies in Applied Mathematics **49**, 21 (1970).
[13] V. F. Kopiev and S. A. Chernyshev, Vortex ring eigen-oscillations as a source of sound, Journal of Fluid Mechanics **341**, 19 (1997).
[14] J. Larsson and S. K. Lele, Direct numerical simulation of canonical shock/turbulence interaction, Phys. Fluids **21**, 126101 (2009).
[15] M. S. Howe, Contributions to the theory of aerodynamic sound, with application to excess jet noise and the theory of the flute, Journal of Fluid Mechanics **71**, 625 (1975).
[16] T. Colonius and S. K. Lele, Computational aeroacoustics: progress on nonlinear problems of sound generation, Progress in Aerospace Sciences **40**, 345 (2004).
[17] D. J. Bodony and S. K. Lele, Current status of jet noise predictions using large-eddy simulation, AIAA Journal **46**, 364 (2008).
[18] L. S. G. Kovasznay, Turbulence in supersonic flow, Journal of the Aeronautical Sciences **20**, 657 (1953).
[19] B.-T. Chu, On the energy transfer to small disturbances in fluid flow (Part I), Acta Mechanica **1**, 215 (1965).
[20] C. L. Morfey, Acoustic energy in non-uniform flows, Journal of Sound and Vibration **14**, 159 (1971).
[21] P. E. Doak, Momentum potential theory of energy flux carried by momentum fluctuations, Journal of Sound and Vibration **131**, 67 (1989).
[22] W. G. Unruh, Experimental black-hole evaporation?, Physical Review Letters **46**, 1351 (1981).
[23] M. Visser, Acoustic black holes: horizons, ergospheres and Hawking radiation, Classical and Quantum Gravity **15**, 1767 (1998).
[24] C. Barceló, S. Liberati, and M. Visser, Analogue gravity, Living Reviews in Relativity **14**, 3 (2011).
[25] M. Mancinelli, T. Pagliaroli, A. Di Marco, R. Camussi, and T. Castelain, Wavelet decomposition of hydrodynamic and acoustic pressures in the near field of the jet, Journal of Fluid Mechanics **813**, 716 (2017).
[26] M. E. Goldstein, A generalized acoustic analogy, Journal of Fluid Mechanics **488**, 315 (2003).
[27] S. Schoder, K. Roppert, and M. Kaltenbacher, Post-processing of direct aeroacoustic simulations using Helmholtz decomposition, AIAA Journal **58**, 3019 (2020).
[28] R. Farwig, H. Kozono, and H. Sohr, On the Helmholtz

decomposition in general unbounded domains, Archiv der Mathematik **88**, 239 (2007).
[29] O. G. Ernst and M. J. Gander, Why it is difficult to solve Helmholtz problems with classical iterative methods, in *Numerical Analysis of Multiscale Problems* (Springer Berlin Heidelberg, Berlin, Heidelberg, 2012) pp. 325–363.
[30] K. Mahesh, S. Lee, S. K. Lele, and P. Moin, The interaction of an isotropic field of acoustic waves with a shock wave, Journal of Fluid Mechanics **300**, 383 (1995).
[31] P. Delorme, P. Mazet, C. Peyret, and Y. Ventribout, Computational aeroacoustics applications based on a discontinuous Galerkin method, Comptes Rendus Mécanique **333**, 676 (2005).
[32] A. D. Pierce, Wave equation for sound in fluids with unsteady inhomogeneous flow, The Journal of the Acoustical Society of America **87**, 2292 (1990).
[33] N. Bilić, Relativistic acoustic geometry, Classical and Quantum Gravity **16**, 3953 (1999).
[34] G. E. Volovik, *The Universe in a Helium Droplet* (Oxford University Press, 2009).
[35] R. Schützhold and W. G. Unruh, Gravity wave analogues of black holes, Physical Review D **66**, 044019 (2002).
[36] C. Park and S. Choi, Covariant Helmholtz–Hodge decomposition: Resolving spurious vorticity via acoustic geometry (2026), arXiv:2602.05399 [physics.flu-dyn].
[37] H. S. Ribner, The generation of sound by turbulent jets, in *Advances in Applied Mechanics*, Advances in Applied Mechanics, Vol. 8, edited by H. L. Dryden and T. von Kármán (Elsevier, 1964) pp. 103–182.
[38] M. Dafermos and Y. Shlapentokh-Rothman, Rough initial data and the strength of the blue-shift instability on cosmological black holes with $\Lambda > 0$, Classical and Quantum Gravity **35**, 195010 (2018).
[39] A. Einstein, Über den Einfluss der Schwerkraft auf die Ausbreitung des Lichtes, Annalen der Physik **340**, 898 (1911).
[40] R. V. Pound and G. A. R. Jr, Apparent weight of photons, Physical Review Letters **4**, 337 (1960).
[41] L. B. Okun, K. G. Selivanov, and V. L. Telegdi, On the interpretation of the redshift in a static gravitational field, American Journal of Physics **68**, 115 (2000).
[42] D. Colton and R. Kress, *Inverse Acoustic and Electromagnetic Scattering Theory*, 4th ed., Applied Mathematical Sciences, Vol. 93 (Springer Nature Switzerland, Cham, 2019).
[43] J. P. Kaipio and E. Somersalo, *Statistical and Computational Inverse Problems*, Applied Mathematical Sciences, Vol. 160 (Springer-Verlag New York, New York, NY, 2005).
[44] S. W. Hawking, Black hole explosions?, Nature **248**, 30 (1974).
[45] J. Steinhauer, Observation of quantum Hawking radiation and its entanglement in an analogue black hole, Nature Physics **12**, 959 (2016).
[46] S. Patrick, H. Goodhew, C. Gooding, and S. Weinfurtner, Backreaction in an analogue black hole experiment, Phys. Rev. Lett. **126**, 041105 (2021).
[47] C.-W. Shu and S. Osher, Efficient implementation of essentially non-oscillatory shock-capturing schemes, II, Journal of Computational Physics **83**, 32 (1989).
[48] G.-S. Jiang and C.-W. Shu, Efficient implementation of weighted ENO schemes, Journal of Computational Physics **126**, 202 (1996).
[49] E. M. Taylor, M. Wu, and M. P. Martín, Optimization of nonlinear error for weighted essentially non-oscillatory methods in direct numerical simulations of compressible turbulence, Journal of Computational Physics **223**, 384 (2007).
[50] J. F. McKenzie and K. O. Westphal, Interaction of linear waves with oblique shock waves, The Physics of Fluids **11**, 2350 (1968).
[51] C. E. Shannon, A mathematical theory of communication, The Bell System Technical Journal **27**, 379 (1948).
[52] T. M. Cover and J. A. Thomas, *Elements of Information Theory*, 2nd ed. (John Wiley & Sons, Inc., Hoboken, New Jersey, 2006).
[53] S. W. Hawking, Breakdown of predictability in gravitational collapse, Phys. Rev. D **14**, 2460 (1976).
[54] R. Brito, V. Cardoso, and P. Pani, Partially massless gravitons do not destroy general relativity black holes, Phys. Rev. D **87**, 124024 (2013).

End Matter

Appendix A: Numerical implementation and benchmark setup— To quantify CCKD leakage independently of truncation artifacts, all differential operators are discretized using mimetic finite-difference operators in a weak (variational) form. In particular, the discrete divergence is realized as the negative adjoint of the discrete gradient under the appropriate metric-weighted inner product, so that the discrete integration-by-parts (adjoint) identities hold to within round-off error.

A.1 Discrete operators, weak-form assembly, and regularization. Spatial derivatives are constructed via Kronecker products of 1D first-derivative matrices (second-order central in the interior with one-sided boundary closure). The covariant Laplace–Beltrami operator is assembled in weak form as a symmetric metric-weighted stiffness operator,

$$(\Delta_\gamma \phi) \;\approx\; \frac{1}{\sqrt{\gamma}}\Big[(-D_x^{\mathsf{T}})\, f_x(\phi) + (-D_y^{\mathsf{T}})\, f_y(\phi)\Big], \qquad (11)$$

where the metric-weighted fluxes are

$$\begin{aligned} f_x(\phi) &= \sqrt{\gamma}\big(\gamma^{xx} D_x\phi + \gamma^{xy} D_y\phi\big), \\ f_y(\phi) &= \sqrt{\gamma}\big(\gamma^{yx} D_x\phi + \gamma^{yy} D_y\phi\big). \end{aligned} \qquad (12)$$

This weak-form (stiffness) construction yields a symmetric (semi-)definite discrete operator and enforces the natural boundary condition through the vanishing of the boundary term arising from discrete integration by parts. In the benchmarks considered here, disturbances are localized, so the resulting natural boundary condition is effectively homogeneous.

For the Helmholtz–Hodge stage we employ the Natural CHHD formulation, i.e. a monolithic variational solve for the potentials (ϕ, Ψ) that enforces the covariant orthogonal decomposition with natural boundary coupling [36].

The scalar potential is determined up to an additive constant; we remove the null space by fixing a gauge (equivalently, pinning a single degree of freedom at a reference point), which leaves $\nabla_\gamma \phi$ unchanged.

For transonic and supersonic regimes (Analogue Black Hole and Shu–Osher), the metric singularity at the horizon ($|U_0| \to c_0$) is regularized by enforcing $\beta_{\text{safe}} = \max(c_0^2 - |\mathbf{U}_0|^2, 10^{-12}\max(c_0^2))$. The resulting sparse symmetric systems are solved with a direct sparse solver (or, equivalently, with a symmetric Krylov method when used) to the stated numerical tolerance.

A.2 Leakage quantification. To quantify the separation fidelity, we define a dimensionless leakage metric $\mathcal{L}$ representing the magnitude of the spurious residual normalized by the physical signal scale. For kinematic leakage (Figs. 1, 2), we normalize the local vorticity residual by the Frobenius norm of the acoustic velocity Jacobian,

$$\mathcal{L}_{\text{vort}} = \frac{|\zeta_{\text{cov}}|}{\|\nabla \mathbf{u}_{\text{ac}}\|_F + \epsilon}. \tag{13}$$

This formulation ensures dimensional consistency and rigorously tests the geometric identity independent of the local velocity magnitude. Conversely, for thermodynamic leakage (Figs. 6, 7), we normalize the spurious acoustic variable by the global peak magnitude of the input entropy,

$$\mathcal{L}_{\text{ent}} = \frac{|q_{\text{ac,spurious}}|}{\max|q_{\text{input}}| + \epsilon}. \tag{14}$$

This metric serves as a direct proxy for the false-positive scattering rate: it measures how much static thermodynamic energy is misidentified as propagating sound solely due to coordinate misalignment.

A.3 Thermal-lens entropy-spot benchmark (2D). The domain is $(x, y) \in [0, 4] \times [-2, 2]$ with 800×800 resolution. The background is a Gaussian thermal lens superposed with a shear flow:

$$\begin{aligned} c_0(x, y) &= 340 + 70\exp\big(-4[(x-2)^2 + y^2]\big), \\ U_0(y) &= 150\tanh(2y), \quad V_0 = 0. \end{aligned} \tag{15}$$

A localized acoustic packet (ϕ) and a stationary entropy spot (s') are prescribed as:

$$\begin{aligned} \phi(x, y) &= \sin(2\pi x)\cos(2\pi y)\exp\left(-\frac{(x-2)^4 + y^4}{1.5}\right), \\ s'(x, y) &= 0.5\exp\big(-10[(x-2)^2 + (y+0.5)^2]\big). \end{aligned} \tag{16}$$

This setup isolates thermodynamic-mode ambiguity in a strongly refracting geometry.

A.4 Analogue black-hole benchmark (2D). The test is performed on $(x, y) \in [-4, 4]^2$ with 800×800 resolution. The background is a rotating draining-vortex flow with drain strength $D = 1.5$ and circulation $C = 2.0$:

$$v_r = -\frac{D}{r}, \quad v_\theta = \frac{C}{r}. \tag{17}$$

The sound speed follows the Bernoulli equation with $H_\infty = 1.0$:

$$c_0^2(r) = gH(r) = gH_\infty - \frac{1}{2}(v_r^2 + v_\theta^2). \tag{18}$$

This generates an acoustic horizon at $|v_r| = c_0$. A spiraling acoustic packet and a horizon-trapped entropy perturbation are superposed to stress the decomposition in near-degenerate metric regions.

A.5 Shu–Osher shock–entropy interaction (1D). We solve the canonical Shu–Osher configuration following the computational setup and boundary conditions detailed by Taylor *et al.* [49]. The problem is solved on $x \in [0, 1]$ with $N = 4800$ uniform finite-volume cells. The flow is governed by the Euler equations with a specific heat ratio $\kappa = 1.4$. The initial condition is a Mach 3 normal shock located at $x_s = 1/8$ separating an exact post-shock state (left) from a pre-shock state (right) with a sinusoidal density modulation (entropy wave):

$$\begin{aligned} (\rho, u, p)(x, 0) &= \begin{cases} (3.857,\ 2.629,\ 10.333), & x < x_s, \\ \big(1 + \alpha\sin[k(x - x_s)],\ 0,\ 1\big), & x \geq x_s, \end{cases} \\ &\text{where} \quad \alpha = 0.2, \quad k = \frac{2\pi}{\lambda}, \quad \lambda = \frac{1}{8}. \end{aligned} \tag{19}$$

Here, the post-shock values are derived from the Rankine–Hugoniot relations for a moving shock with $M = 3.0$. Time integration uses an explicit RK4 scheme with a CFL number of 0.5, and spatial fluxes are computed using a WENO5 reconstruction with Lax–Friedrichs-type splitting. Zero-gradient boundary conditions are applied at both ends. The simulation is advanced to $t_{\text{end}} = 0.21\, L/a_R$ to capture shock-driven entropy-acoustic conversion.

Appendix B: Supplementary validation and interpretation: Geometric robustness of the covariant projection—

This appendix provides supplementary checks of the covariant projection in refractive and transcritical geometries where Euclidean post-processing can be sensitive to metric effects. We emphasize two criteria: (i) *thermodynamic robustness*—stationary entropy should remain non-propagating under post-processing, and (ii) *signal fidelity*—the propagating acoustic component should be preserved without suppressing genuine high-frequency content induced by geometric compression.

B.1 Thermodynamic robustness: entropy spot in curved backgrounds. We consider a stationary entropy

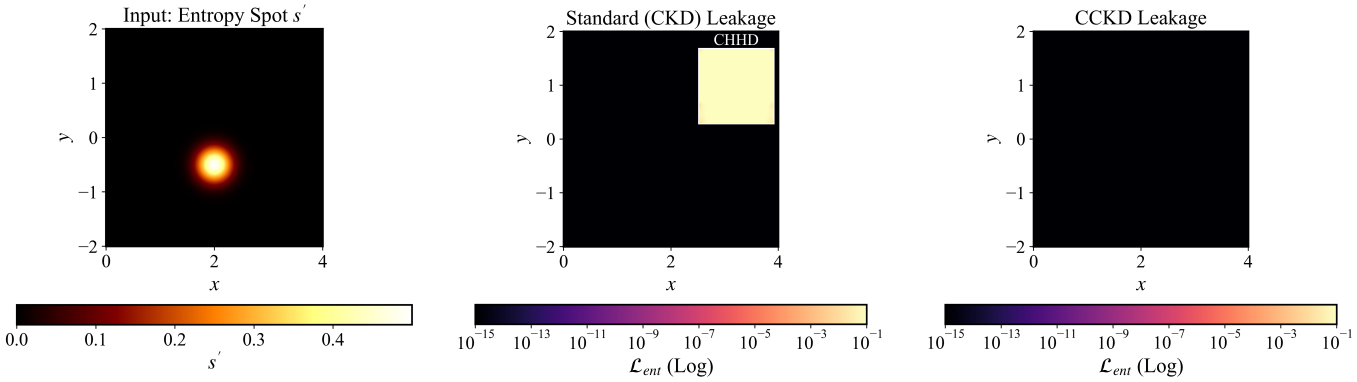

(a) Input entropy spot s'.

(b) Standard (Euclidean) leakage magnitude.

(c) Covariant thermodynamic leakage magnitude.

FIG. 6: Thermodynamic isolation in a thermal lens (supplementary). The entropy spot is non-propagating; the standard CKD baseline is already accurate due to explicit thermodynamic separation, while the covariant projection provides a metric-aligned reference at the numerical floor.

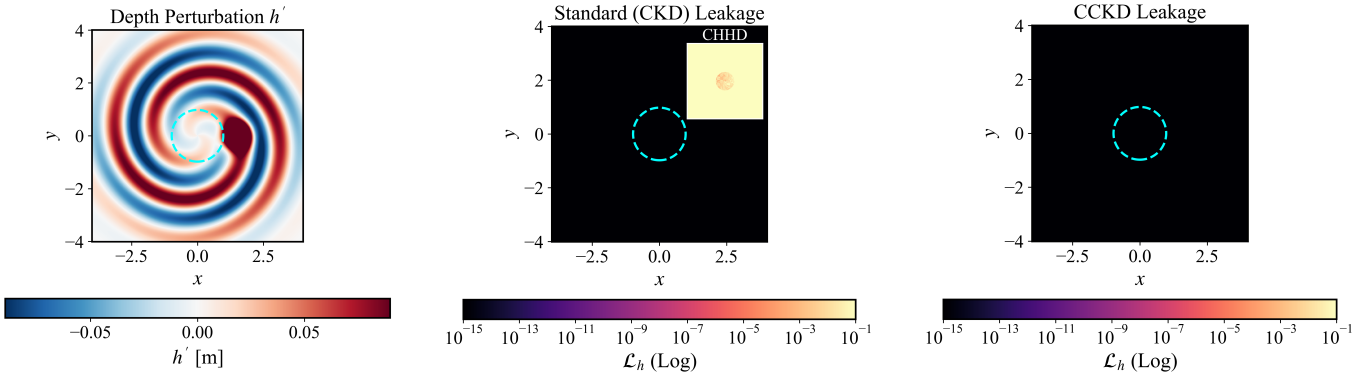

(a) Depth perturbation h' (thermodynamic/noise proxy).

(b) Standard (Euclidean) entropy leakage.

(c) Covariant thermodynamic leakage.

FIG. 7: Thermodynamic diagnostic near an analogue black hole (supplementary). A trapped thermodynamic perturbation should not appear as outgoing sound; CKD is already robust, and the covariant projection remains consistent as a metric-aligned reference in the transcritical geometry.

fluctuation embedded in an inhomogeneous background (Appendix A). Since CKD already isolates entropy before the velocity split, thermodynamic separation is not limiting here (Fig. 6); we include this case only as a consistency check that non-propagating entropy is not misidentified as sound in a refractive geometry.

B.2 Analogue black-hole benchmark: fidelity stress test at a horizon. Similarly, CKD remains effective at isolating stationary thermodynamic content in this configuration (Fig. 7). We therefore use the analogue black-hole geometry mainly as a fidelity check: near the horizon the effective metric becomes near-degenerate, so Euclidean diagnostics can become ill-conditioned, and the key question is whether the covariant projection restores the propagating acoustic component without suppressing genuine near-horizon high-frequency content (Fig. 8).

B.3 Mode restoration from a mixed snapshot. To test signal fidelity, we prescribe a synthetic Hawking-style superposition: a weak, spiraling acoustic packet embedded in a high-amplitude stationary thermodynamic disturbance trapped at the horizon. From the mixed field, the covariant projection restores the propagating acoustic component while relegating non-propagating content to the thermodynamic residual (Fig. 8). Importantly, the extracted acoustic signal retains the expected near-horizon blue-shifting signature (wavelength compression) without misclassifying true high-frequency content as noise. This demonstrates that the method is not merely a denoiser but a geometry-consistent projector that separates modes by causal character (radiative vs. trapped) in the regime where Euclidean diagnostics fail.

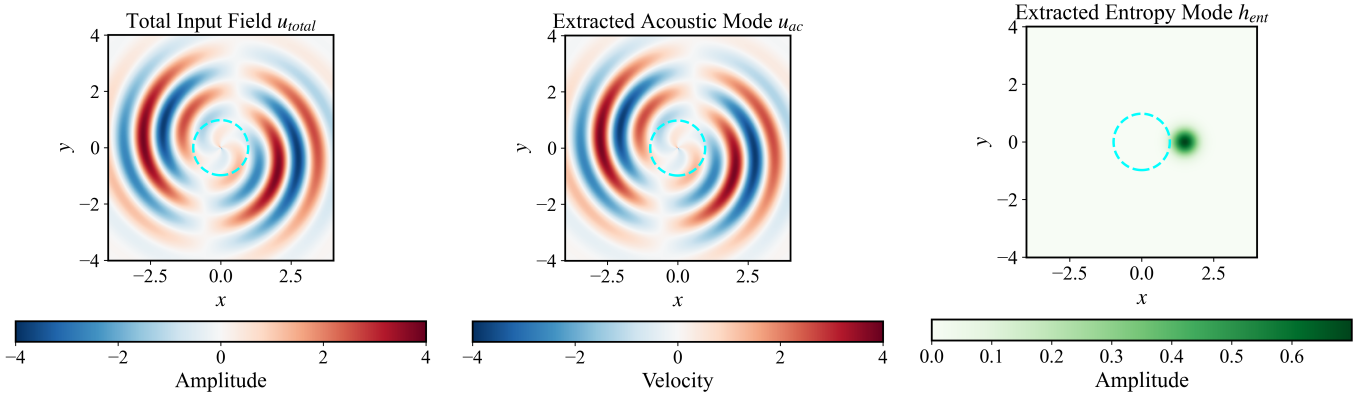

(a) Total input field u_{total}. (b) Extracted acoustic mode u_{ac}. (c) Extracted thermodynamic mode h_{ent}.

FIG. 8: Mode restoration in the analogue black-hole benchmark. From a mixed signal+noise snapshot, the covariant thermodynamic projection returns the propagating acoustic component and isolates the trapped thermodynamic residual.

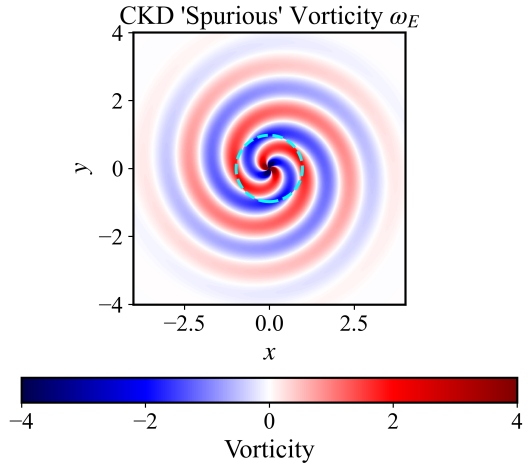

FIG. 9: Geometric illusion: Euclidean CKD spurious vorticity ω_E. Apparent vortical structure arises from applying Euclidean operators to a curved acoustic manifold in the analogue black-hole geometry.

B.4 Geometric illusion in Euclidean diagnostics. For completeness, Fig. 9 plots the raw Euclidean vorticity diagnostic $\omega_E = \partial_x v - \partial_y u$ computed directly from the prescribed (vorticity-free) acoustic packet. The coherent spiral pattern is therefore not physical rotation but a coordinate/metric illusion induced by applying flat-space derivatives in the transcritical geometry, where refraction and near-horizon shear imprint curvature onto Euclidean gradients. This same illusion is what drives the Euclidean vorticity-leakage reported in Fig. 2.

Appendix C: Theoretical basis of geometric blue-shift— The spectral compression observed in Fig. 5 is not a kinematic coincidence but a direct consequence of wave propagation on a stationary acoustic metric [23, 24]. In the shock-attached frame, the background flow is time-independent, admitting a timelike Killing vector field $\xi^\mu = (\partial_t)^\mu$. The propagation of fluctuations is governed by the effective acoustic metric $g_{\mu\nu}$, which in (t, x) coordinates takes the Schwarzschild-like form

$$ds^2 = g_{\mu\nu}dx^\mu dx^\nu = \frac{\rho_0}{c_0}\left[-(c_0^2 - u_0^2)\,dt^2 + \dots\right]. \quad (20)$$

For high-frequency (WKB) perturbations, the phase gradient defines a 4-wavevector K_μ; stationarity implies conservation of the Killing frequency $\Omega = -\xi^\mu K_\mu$, representing the energy observed by a stationary observer at infinity. Across the shock, this conserved frequency links the upstream entropy mode ($\mathcal{S}$) and downstream acoustic mode ($\mathcal{P}$):

$$\omega_{\mathcal{S}} = \omega_{\mathcal{P}}. \quad (21)$$

The magnitude of the wavenumber shift is dictated by the distinct dispersion relations (null geodesics) of the two mode families. The incident entropy mode follows the convective path $\omega = U_1\, k_{\mathcal{S}}$, while the scattered acoustic mode propagates along the null cone of the downstream metric, yielding $\omega = (c_2 - U_2)\, k_{\mathcal{P}}$, where U_1 is the upstream convective speed in the shock-attached frame and U_2, c_2 are the downstream mean velocity and sound speed, respectively. Combining these with Eq. (21) yields the geometric blue-shift ratio [38]:

$$\Lambda \equiv \frac{k_{\mathcal{P}}}{k_{\mathcal{S}}} = \frac{U_1}{c_2 - U_2} = \frac{M_1\sqrt{\chi}}{1 - M_2}. \quad (22)$$

Here M_1 and M_2 are the upstream and downstream Mach numbers in the shock-attached frame, and $\chi \equiv T_1/T_2$ is the static temperature ratio determined by the Rankine–Hugoniot relations. This shift Λ is the acoustic analogue of the gravitational redshift $z + 1 = \sqrt{g_{00}(r_1)/g_{00}(r_2)}$ [23]. Thus, the shock acts as a thermo-acoustic spectral magnifier: it maps an entropy fluctuation at wavelength λ into an acoustic fluctuation at the

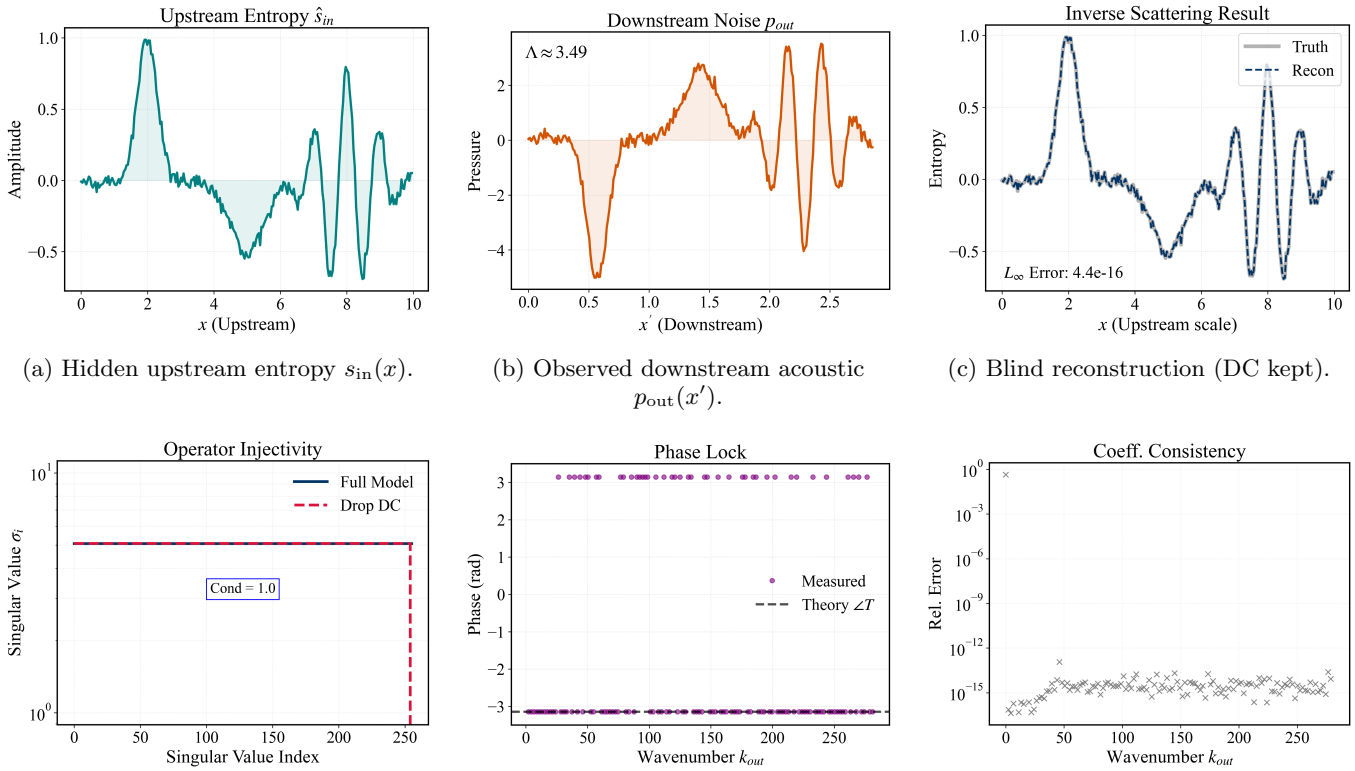

(a) Hidden upstream entropy $s_{\text{in}}(x)$.

(b) Observed downstream acoustic $p_{\text{out}}(x')$.

(c) Blind reconstruction (DC kept).

(d) Injectivity: full rank vs. drop-DC.

(e) Phase lock on energetic modes.

(f) Coefficient consistency (rel. error).

FIG. 10: Holography validation ($M_1 = 3$ LIA benchmark). The shock acts as a unitary operator on the retained subspace. (d) The map is full-rank if the DC mode is tracked. (a–c) Inverting the blue-shifted acoustic trace recovers the upstream entropy to machine precision, confirming the shock is a deterministic information channel.

finer scale λ/Λ, consistent with the wavenumber increase observed in Fig. 5.

Appendix D: Shock-wave holography: Information-preserving scattering—

This appendix validates the operator-theoretic claim that a steady normal shock acts as a deterministic, information-preserving channel in the idealized linear setting. We utilize a Linearized Interaction Analysis (LIA) benchmark fixed to the Mach-3 Rankine–Hugoniot background [9]. Unlike the spatially extended Shu–Osher simulation, this compact-shock framework allows for exact spectral diagnostics of the scattering map.

We discretize the linearized map relating upstream entropy coefficients to downstream acoustic coefficients as a linear system $\mathbf{y} = \mathbf{A}\mathbf{x}$, where $\mathbf{x} = \{\hat{s}_{\text{in}}(k_m)\}_{m=1}^{N}$ and $\mathbf{y} = \{\hat{p}_{\text{out}}(k_m)\}_{m=1}^{N}$ collect the Fourier coefficients (in the shock-normal direction) of the incident entropy signal and the transmitted acoustic pressure, respectively. Analytically, this forward operator induces a spectral dilation. Consequently, the inverse operator $\mathbf{A}^{-1}$ is given explicitly by the Holographic Inverse Law:

$$\hat{s}_{\text{in}}(k) \;=\; \mathcal{T}^{-1}(k)\,\hat{p}_{\text{out}}(\Lambda k)\,e^{-i\Delta\varphi(k)}, \qquad (23)$$

where k is the wavenumber, $\Lambda \equiv k_{\text{out}}/k_{\text{in}} > 1$ is the geometric blue-shift factor, $\mathcal{T}(k)$ is the transmission magnitude, and $\Delta\varphi(k)$ is the corresponding phase delay determined by the Rankine–Hugoniot boundary conditions.

The singular value spectrum (Fig. 10d) confirms that the discretized operator $\mathbf{A}$ is full-rank and invertible on the retained subspace, provided the mean (DC, $k = 0$) mode is included; explicitly dropping the DC mode introduces a single null direction. To demonstrate this invertibility, we perform a blind reconstruction (Fig. 10a–c). A multi-scale entropy signal is propagated through the shock model, generating a high-frequency acoustic trace. Applying the inverse operator $\mathbf{x} = \mathbf{A}^{-1}\mathbf{y}$ (implementing Eq. (23)) recovers the input signal to floating-point precision ($\sim 10^{-15}$). Spectral diagnostics (Fig. 10e–f) confirm that the recovery is highly effective within the primary signal bandwidth, maintaining robust phase locking across the energetic wavenumbers. Crucially, the recovered phase faithfully tracks the deterministic shift $\Delta\varphi(k)$, accurately capturing the characteristic π-phase inversion (sign flip) predicted by the shock's negative transmission coefficient.